Journal of Materials Science: Materials in Electronics (2020) 31:7946–7952
https://doi.org/10.1007/s10854-020-03333-7

Magnetoresistive effect in the cobalt-doped bismuth ferrite films

O. B. Romanova[1] · S. S. Aplesnin[1,2] · M. N. Sitnikov[2] · L. V. Udod[1,2] · O. B. Begisheva[2] · O. F. Demidenko[3]

Received: 6 February 2020 / Accepted: 27 March 2020 / Published online: 8 April 2020

Abstract
Bismuth ferrite films have been synthesized by the burst-mode deposition of the $BiFe_{0.8}Co_{0.2}O_3$ solid solutions onto object glasses. The surface morphology of the $BiFe_{0.8}Co_{0.2}O_3$ films has been examined. The effect of electron doping implemented by substitution of cobalt for iron in the $BiFe_{0.8}Co_{0.2}O_3$ films on their magnetic, electrical, and galvanomagnetic properties has been investigated at temperatures of 77−600 K in magnetic fields of up to 12 kOe. The negative magnetoresistance has been observed, which changes its sign in the region of formation of magnetically heterogeneous states and attain its maximum value above room temperature. It has been established that the magnetoresistance is caused by the competition of electron hoppings and localization of electrons in a magnetic field. Using the Hall measurements, the carrier type has been determined. A model of the change in the curriers sign upon heating due to the shift of the chemical potential relative to the impurity subband has been proposed.

1 Introduction

Multiferroics are promising for solving applied problems of modern engineering as materials for electronic elements [1, 2]. The interplay of the electric and magnetic subsystems in multiferroics, which manifests itself as the magnetoelectric effect, makes it possible to manipulate the magnetic properties of the materials by an electric field and, vice versa, change their electrical properties by a magnetic field. The $BiFeO_3$ (BFO) compound is one of the most wide-spread materials currently used in data processing and storage devices due to its bright room temperature magnetoelectric properties and the high temperature of the phase transitions, including ferroelectric one occurring at $T_C = 1143$ K and antiferromagnetic one observed at $T_N = 643$ K [3, 4]. The BFO crystal structure is described well by the rhombohedral space group $R3c$. The low-temperature ($T = 140.3$ K) surface phase transition observed in the BFO nanotubes was accompanied by a drastic change in the lattice parameter and surface charge density [5]. The BFO compound is characterized by the G-type short-range antiferromagnetic order, in which the Fe^{3+} ion is surrounded by six ions with the opposite spin orientation [6]. The BFO magnetic structure represents a spin cycloid with a wave period of $k = (0.0045, 0.0045, 0)$ or a period of about 620 ± 20 Å. The magnetic moments of iron ions rotate in the (110) plane along the [110] direction of the cycloid [7]. The suppression of the spin cycloid by adding the 3d and 4f impurities and the transition from bulk samples to thin films in bismuth ferrite enhance the magnetoelectric effect [8–11]. The coexistence of the magnetoelectric effect and conductivity makes it possible to control the current by both magnetic and electric field [12]. The giant magnetoresistance (GMR) properties can be very useful for application, e.g., in magnetoresistive sensors and magnetic read heads. A significant GMR value was detected in the Co/Cu, CoFe/Cu, NiFe/Cu, NiCo/Cu, and other film multilayers [13–15]. The value of the effect was found to depend on the layer thicknesses or concentration of, e.g., Fe, in the CoFe/Cu films [16–18].

The electrical properties of the BFO multiferroics can be changed by doping the material with lanthanum (La), samarium (Sm), chromium (Cr), manganese (Mn), lead (Pb), titanium (Ti), niobium (Nb), holmium (Ho), strontium (Sr), etc. [19, 20]. The Sr doping qualitatively changes the ac conductivity of the material. It was established that the conductivity is implemented via electron hoppings over oxygen defects, and the critical concentration of the transition to the

✉ O. B. Romanova
rob@iph.krasn.ru

[1] Kirensky Institute of Physics, Federal Research Center KSC SB RAS, Krasnoyarsk, Russia 660036

[2] Siberian State University of Science and Technology, Krasnoyarsk, Russia 660014

[3] Scientific-Practical Materials Research Center, National Academy of Science of Belarus, 220072 Minsk, Belarus

metal state was determined [21]. The La doping turns the $BiLaFe_2O_6$ system into an insulator with a bandgap narrower than in the initial BFO compound [22].

The substitution of manganese for iron in the BFO system leads to the formation of a half-filled impurity subband located above the valence band by 0.9 eV, according to the local density approximation (LDA) calculation of the $[Bi_{16}(Fe_{15}Mn)O_{48}]$ cluster with the rhombohedral symmetry R3 [23]. The Mn doping increases the conductivity described using of the polaron model [24]. In the $BiMn_XFe_{1-X}O_3$ films, the migration-type electric polarization was found, which is related to the space charge accumulation on the crystal and magnetic domain walls [24]. The diode effect found in the $BiMn_XFe_{1-X}O_3$ system in the infra-red (IR) range is caused by the asymmetry of quantum wells resulting from the electric polarization of the film and band bending at the film surface. The difference between the times of carrier thermalization and electron and hole recombination in quantum wells leads to the formation of the *p–n* junction under the IR irradiation [25]. The Mn doping improves the room temperature ferroelectric polarization and magnetoelectric coupling.

The dielectric properties of the cluster glass, nanoparticles, and films with Fe partially replaced by Co ($BiFe_{0.95}Co_{0.05}O_3$) were studied [26–29]. The chemical substitution significantly affects the magnetic and dielectric properties of $BiFeO_3$, since it breaks the cycloidal spin and ensures the high permittivity and magnetization. The multilayer films can be fabricated by electrodeposition, which is one of the most flexible techniques due to its low cost [30, 31]. In [32], the $BiFe_{0.95}Co_{0.05}O_3$ films were made to form on the Pt/Ti/SiO2/Si(111) substrates by chemical solution deposition (CSD). These films exhibited a significantly lower leakage current as compared with that in the pure BFO samples. However, a drawback of this method is the presence of secondary phases. Therefore, the novelty of our work consists in the choice of a method for synthesizing thin films (the burst-mode deposition of the solid solutions onto object glasses) and studying the galvanomagnetic properties of the films with the high substitution concentration.

The aim of this study is to establish the magnetoresistive effect in the electron-doped BFO multiferroics. Electron doping was implemented by the substitution of cobalt ions for iron ones with an additional electron in the t_{2g} shell. In the model of strong electron correlations, this corresponds to the filling of the upper Hubbard subband. The maximum concentration of current carriers can be obtained within one crystal structure of the BFO in the region of the critical concentration of the crystalline phase transition.

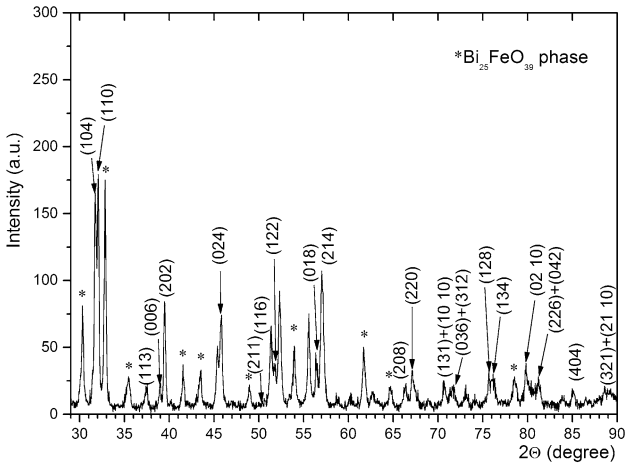

Fig. 1 XRD pattern of the $BiCo_XFe_{1-X}O_3$ ($X=0.2$) film at $T=300$ K

2 Experimental data and discussion

The cobalt-doped bismuth ferrite films were obtained by the burst-mode deposition of the synthesized $BiFe_{0.8}Co_{0.2}O_3$ solid solutions onto object glasses. The $BiFe_{1-X}Co_XO_3$ compositions were prepared from high-purity Fe, Co, and Bi_2O_3. The stoichiometric amounts of the initial components were dissolved in diluted (1:1) nitric acid evaporated to wet salts. Then, they were dissolved in water and a mixture (aqueous solution) of bismuth, cobalt, and manganese nitrates was obtained. The solution of citric acid and ethylene glycol was used as a gelling agent, which was added to the solution of the stoichiometric amounts of the nitrates. Organic compounds were removed by heating the product to 450 °C. After that, bulk samples in the form of tablets with a diameter of 8 mm and a thickness of 1.5 mm were obtained by crushing the powders and subjecting them to cold isostatic pressing (~ 2 kbar), followed by annealing at 850 °C for 10 min. To obtain precursors, the bulk tablets were ground into polycrystalline powders with a grain size from 0.1 to 0.3 mm.

The films were deposited in a UVN-71R-2 vacuum facility. The pressure in a reaction chamber during deposition was 10^{-3} Pa and the temperature of a tantalum evaporator was kept around 2000 °C. The substrates were placed at a distance of 10 cm from the evaporator and their temperature was changed between 250 and 300 °C. The films were 13×17 mm in size and had a thickness of 660 nm. The phase composition and crystal structure of the synthesized $BiFe_{0.8}Co_{0.2}O_3$ films were examined on a DRON-3 X-ray diffractometer (CuK_α radiation) at 300 K in the pointwise data accumulation mode. According to the X-ray diffraction data, the main phase of the synthesized samples is the $BiFe_{1-X}Co_XO_3$ (BFCO) compound with the

rhombohedral structure (sp. gr. *R3c*) and crystal lattice parameters of $a = b = 0.558$ nm and $c = 1.380$ nm (Fig. 1). Along with the main BFCO phase, the X-ray diffraction pattern contains reflections (marked by the asterisk in the figure) corresponding to the $Bi_{25}FeO_{39}$ paramagnetic phase with a selenite structure (more than 5%) [33].

The surface morphology of the $BiFe_{0.8}Co_{0.2}O_3$ films was examined by scanning electron microscopy (SEM) on a Hitachi SU3500/Model3500 microscope and a Hitachi S-5500 high-resolution electron microscope. The microstructure of the samples was characterized on a Hitachi HT7700 transmission electron microscope (TEM).

The enlarged SEM images of the $BiFe_{0.8}Co_{0.2}O_3$ film surface are presented in Fig. 2. The qualitative and semi-quantitative composition of the samples was determined (Table 1). The semi-quantitative composition of the samples studied on a SEM microscope was found to be consistent with the expected presence of Co ions in the $BiFe_{0.8}Co_{0.2}O_3$ samples. The elemental composition of the investigated film is given in Table 1. The elemental mapping in the wave and energy dispersion modes reflects the distribution of elements in the sample. According to the morphological analysis, coarser grains with wide intergrain spacings were observed for the pure BFO thin film

Table 1 Spectrum: pointwise semiquantitative analysis

Element	AN	Series	norm. C (wt. %)	Atom. C (at. %)
Bismuth	83	L-series	79.75	29.6
Oxygen	8	K-series	12.25	59.4
Iron	26	K-series	6.59	9.16
Cobalt	27	K-series	1.4	1.85
		Total	100	100

[34]. The Co doping of BFO significantly affects the morphology of the $BiFe_{0.8}Co_{0.2}O_3$ thin films. A similar situation was observed in the multilayer films containing nickel. The Ni content influenced the surface morphology of the multilayer films [35]. The morphology images (Fig. 2) show that the grain boundaries in the $BiFe_{0.8}Co_{0.2}O_3$ samples are significantly reduced as compared with the original BFO compound. A decrease in the grain microparticles can improve the electrical properties of the samples. The surface of the spray-deposited $BiFe_{0.8}Co_{0.2}O_3$ films is

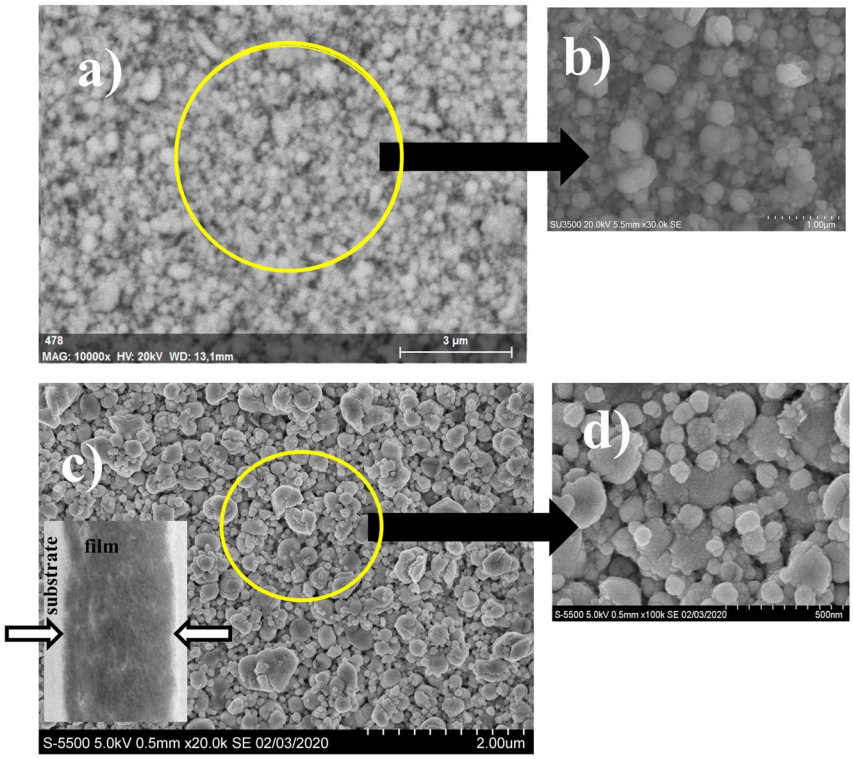

Table 1. Spectrum: Pointwise semi-quantitative analysis

Element	AN	Series	norm. C [wt.%]	Atom. C [at.%]
Bismuth	83	L-series	79,75	29,60
Oxygen	8	K-series	12,25	59,40
Iron	26	K-series	6,59	9,16
Cobalt	27	K-series	1,40	1,85
		Total:	100,00	100,00

Fig. 2 SEM images of the $BiCo_{0.2}Fe_{0.95}O_3$ film obtained on a Hitachi SU3500/Model3500 SEM with resolutions of **a** 10000x HV:20 kV and **b** 20.0 kV 5.5 mm x 30.0 k and on a Hitachi S-5500 high-resolution electron microscope with resolutions of (**c**) 5.0 kV 0.5 mm x20.0 k and (**d**) 5.0 kV 0.5 mm x 100 k. Inset in (**c**): TEM images of the $BiCo_{0.2}Fe_{0.95}O_3$ film obtained on a Hitachi 7700 microscope and the film cross-section. Table 1 pointwise semi-quantitative analysis

highly smooth, which is confirmed by the TEM data. The cross-sectional images of the $BiFe_{0.8}Co_{0.2}O_3$ thin films are shown in the inset to Fig. 2c. The analysis of the cross-sectional TEM images showed that thickness of the films on glass substrates is about 660 nm.

The magnetization (M) of the $BiFe_{0.8}Co_{0.2}O_3$ film was measured by the Faraday method in the temperature range of 77−600 K in a magnetic field of 8.6 kOe (Fig. 3). The temperature dependence of magnetization has a small maximum near 360 K, which is caused by the formation of a magnetic inhomogeneity. Upon heating above this temperature, the magnetization smoothly decreases and tends to zero at 600 K, which corresponds to the temperature of the magnetic phase transition. The formation of a magnetic inhomogeneity is caused by the destruction of the spin cycloid.

The substitution of cobalt for iron forms electrically heterogeneous states, including the local electric polarization regions. The trend to the formation of inhomogeneous electronic states below the temperature of the magnetic phase transition will lead to the change in the electrical properties as a result of the chemical potential shift. The resistivity and I–V characteristics were measured on the samples by dc two- and four-contact methods in zero field and in a field of 12 kOe. The temperature dependence of the resistivity of the polycrystalline $BiFe_{0.8}Co_{0.2}O_3$ film at $H = 0$ is presented in Fig. 4. In the low-temperature region, the $\rho(T)$ dependence has a minimum caused by the surface phase transition observed in the initial BFO compound [11]. As the temperature increases, the resistivity grows due to the carrier scattering by magnetic inhomogeneities.

The effect of the magnetic field on the transport characteristics of the samples was studied using the field dependences and I–V characteristics measured in zero magnetic field and in a field of 12 kOe at fixed temperatures between

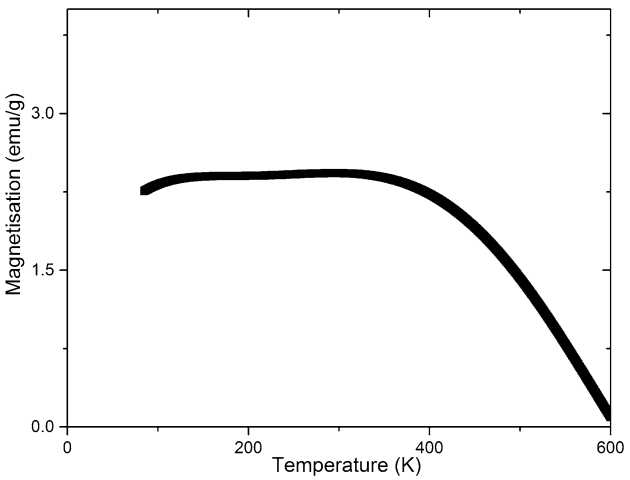

Fig. 3 Temperature dependence of the magnetization for the $BiCo_{0.2}Fe_{0.95}O_3$ film in a magnetic field of $H = 8.6$ kOe

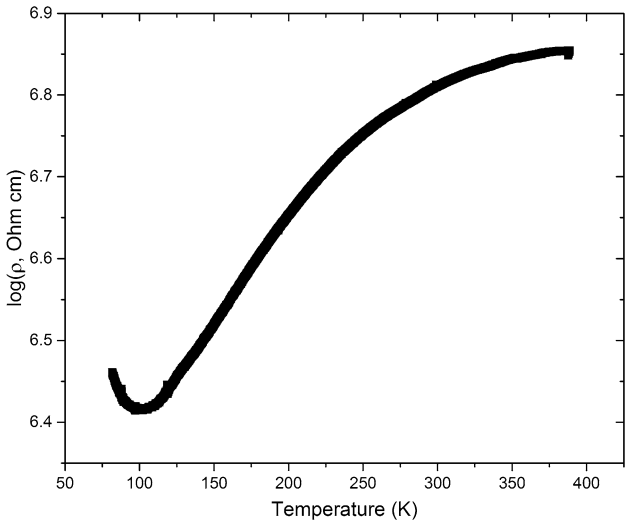

Fig. 4 Temperature dependence of the electrical resistivity for the $BiCo_XFe_{1-X}O_3$ ($X = 0.2$) sample in zero magnetic field

80−390 K. Figure 5 presents field dependences of the magnetoresistance measured at $T = 300$, 330, 360, and 390 K. In the temperature range of 340−370 K, the magnetoresistance changes its sign from negative to positive, which is consistent with the temperature of the maximum magnetization. Upon approaching the temperature of the magnetic phase transition, the negative magnetoresistance increases in the absolute value. A significant contribution to the negative magnetoresistance will be made by hoppings of electrons over the lattice with the matrix elements depending on the mutual orientation of spins on the sites. The hopping probability increases when the magnetic

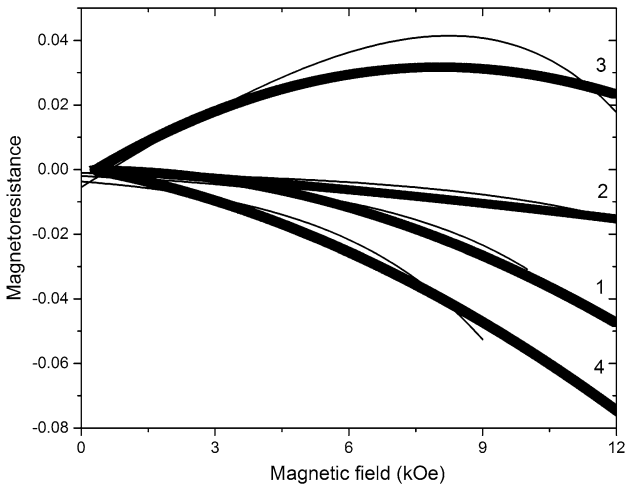

Fig. 5 Field dependence of the magnetoresistance $\delta_H = \frac{R(H)-R(0)}{R(0)}$ for film $BiCo_{0.2}Fe_{0.95}O_3$ at (1) 300K, (2) 330K, (3) 360K and (4) 390K. The solid line shows fitting by Eq. (1) at temperatures of 300, 330, and 390 K and by Eq. (2) at 360 K

Table 2 Magnetoresistance in an electric field of 600 V/cm

T (K)	δ_H (%)
80	2.5
300	− 0.11
330	0.04
390	− 0.38

moments are parallel and decreases at their other directions. The field dependence of the negative magnetoresistance is described by the function [36]

$$(\rho(H) - \rho(0))/\rho(0) = \exp\left(-BH\xi/k_B T\right) - 1 \quad (1)$$

where B is determined by the combination of the energy of the Coulomb interaction of electrons in the impurity band, H is the external magnetic field, and ξ is the electron localization radius.

The smooth growth of the resistance in a magnetic field at temperature 360 K is caused by the formation of magnetically heterogeneous states. In the local region of film with the maximum magnetization, electrons can localize with the formation of the Landau levels [37]. The existence of domain walls with the high carrier mobility leads to the linear dependence of the resistance on the magnetic field [38]. The magnetoresistance is governed by the two mechanisms and expressed as

$$(\rho(H) - \rho(0))/\rho(0) = -1 + \exp\left(-BH\xi/k_B T\right) + aH \quad (2)$$

where a is the fitting parameter. This model satisfactorily describes the experimental data and the maximum magnetoresistance is related to the competition between the hopping mechanism of electrons and their localization.

The I–V characteristics reveal a slight nonlinearity and their slope changes with increasing temperature. The relative change in the resistance (δ_H) calculated using the formula $\delta_H = \frac{R(H)-R(0)}{R(0)}$, where $R(H)$ is the electrical resistance in a magnetic field and $R(0)$ is the resistance without field are given in Table 2. The growth of the electric field by two orders of magnitude leads to a significant decrease in the magnetoresistance absolute value due to the stronger delocalization of carriers and an increase in the carrier mobility.

The observed difference of the behavior of the magnetization and magnetotransport properties from those of the initial BFO compound is caused by the microstructure variation induced by doping with Co ions. A similar difference was observed in the multilayer films in [39].

The carrier type was determined using the Hall measurements. The Hall voltage (U_X) was measured in the temperature range of 100−400 K in a magnetic field of 12 kOe (Fig. 6). In the measurements, the spurious internal voltages

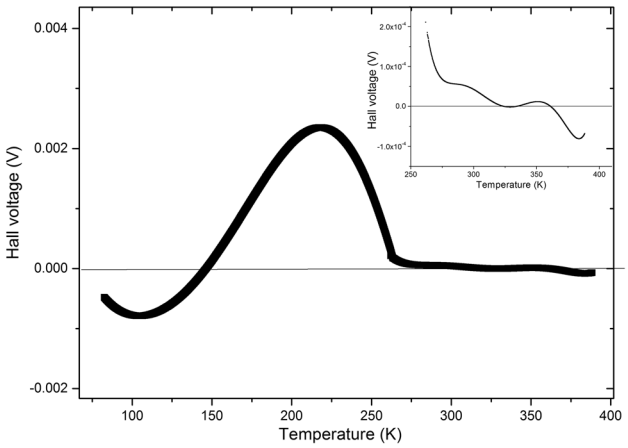

Fig. 6 Temperature dependence of the Hall voltage U_X for the $BiCo_XFe_{1-X}O_3$ ($X = 0.2$) sample. Inset: the change in U_X in the temperature range of 250−380 K

induced by side galvano- and thermomagnetic effects and the asymmetry of contacts were taken into account. The change in the Hall voltage sign from negative to positive in the temperature range of 150−360 K was established. If the product $n\mu_n = p\mu_h$ of the concentration and mobility is independent of the carrier type, at $T = 360$ K the positive magnetoresistance and maximum in the temperature dependence of magnetization are observed. In the low-temperature region, the temperature corresponding to the minimum Hall voltage coincides with the temperature of the surface phase transition, which is indicative of an increase in the concentration and mobility of electrons as compared with those of holes [5]. The Hall voltage passes through the positive maximum at $T = 220$ K, which is apparently related to the change in the position of the chemical potential in the impurity region.

In heterogeneous semiconductors with the Coulomb potential fluctuations, the conductivity is determined by positioning of the chemical potential between the impurities subbands for electrons and holes (Fig. 7a, b). In the polycrystalline $BiFe_{0.8}Co_{0.2}O_3$ film with the high cobalt content, the impurity subband forms from cobalt ions and the position of the chemical potential changes with temperature. We present the electron spectrum consisting of the valence band, conduction band, and impurity subbands at temperatures below and above 200 K. At $T < 200$ K, the chemical potential lies in the upper part of the impurity subband closer to the conduction band edge, which is qualitatively confirmed by the Hall measurement data and maximum growth of the resistance (Fig. 7). Upon heating above 200 K (Fig. 7b), the chemical potential shifts to the bandgap center due to the change in the magnetic state of the film and the transport properties are determined by the transition from the valence band to the hole-type impurity band.

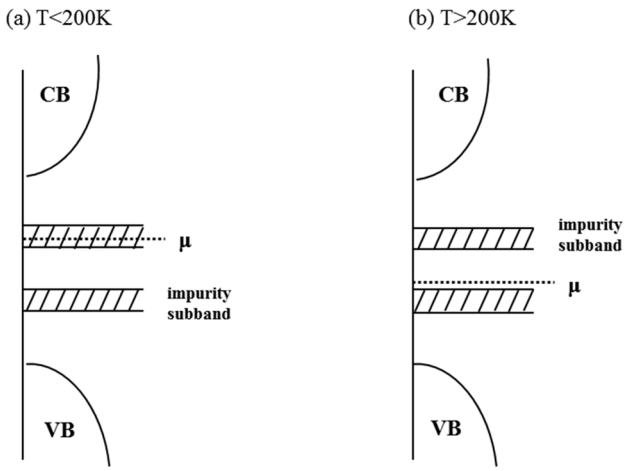

Fig. 7 Electron spectrum consisting of the valence band (VB), conduction band (CB), impurity subbands, and chemical potential (μ) for the $BiCo_{0.2}Fe_{0.95}O_3$ sample at **a** $T < 200$ K and **b** $T > 200$ K

3 Conclusion

The magnetoresistive effect near the critical concentration $X_{cr} = 0.2$ of the structural transition in the $BiFe_{1-X}Co_XO_3$ system with the multiferroic properties was established. The microstructure of the $BiFe_{1-X}Co_XO_3$ thin film were found to be significantly affected by doping with Co ions. The correlation of the maximum magnetoresistance and magnetization temperatures was found. It was shown that, in this temperature range, the resistance increases in a magnetic field, which is caused by the competition between electron hoppings and localization of electrons with the formation of the Landau levels. The carrier type responsible for the positive and negative magnetoresistance was determined.

Acknowledgements The surface morphology of the thin films was examined using methods (SEM and TEM) by the Krasnoyarsk Regional Center of Research Equipment of Federal Research Center "Krasnoyarsk Science Center SB RAS". The reported study was funded by RFBR and BRFBR, Project Number o. 18-52-00009 Bel_a. The reported study was partially funded by Russian Foundation for Basic Research, Government of Krasnoyarsk Territory, Krasnoyarsk Regional Fund of Science № 18-42-240001 r_a, to the research project: «Inversion of the sign of the components of the magnetoelectric tensor on the temperature in films of bismuth garnet ferrite replaced by neodymium».

Author contributions SSA and OBR supervised the experimental work. MNS, LVU, OBB, OFD performed all experimental work. The manuscript was written and discussed by all authors.

References

1. M. Fiebig, J. Phys. D **38**, R123 (2005)
2. J.F. Scott, J. Mater. Chem. **22**, 4567 (2012)
3. S.H. Baek, H.W. Jang, C.M. Folkman, Y.L. Li, B. Winchester, J.X. Zhang, Q. He, Y.H. Chu, C.T. Nelson, M.S. Rzchowski, X.Q. Pan, R. Ramesh, L.Q. Chen, C.B. Eom, Nat. Mater. **9**, 309 (2010)
4. I. Jung, J.Y. Son, Carbon **50**, 3854 (2012)
5. R. Jarrier, X. Marti, J. Herrero-Albillos, P. Ferrer, R. Haumont, P. Gemeiner, G. Geneste, P. Berthet, T. Schülli, P. Cevc, R. Blinc, S.S. Wong, P. Tae-Jin, M. Alexe, M.A. Carpenter, J.F. Scott, G. Catalan, B. Dkhil, Phys. Rev. B **85**, 184104 (2012)
6. J.M. Moreau, C. Michel, R. Gerson, W.J. James, J. Phys. Chem. Solids **32**, 1315 (1971)
7. I. Sosnowska, T.P. Neumaier, E. Steichele, J. Phys. C **15**, 4835 (1982)
8. A.F. Popkov, M.D. Davydova, K.A. Zvezdin, S.V. Solov'yov, A.K. Zvezdin, Phys. Rev. B **93**, 094435 (2016)
9. V.A. Khomchenko, I.O. Troyanchuk, D.V. Karpinsky, S. Das, V.S. Amaral, M. Tovar, V. Sikolenko, J.A. Paixao, J. Phys. D **112**, 084102 (2012)
10. D.V. Karpinsky, I.O. Troyanchuk, M. Tovar, V. Sikolenko, V. Efimov, A.L. Kholkin, J. Alloys Compd. **555**, 101 (2013)
11. J. Li, J. Wang, M. Wutting, R. Ramesh, N. Wang, B. Ruette, A.P. Pyatakov, A.K. Zvezdin, D. Viehland, Appl. Phys. Lett. **84**, 5261 (2004)
12. Y.K. Fetisov, G. Srinivasan, Appl. Phys. Lett. **88**, 143503 (2006)
13. M. Safak, M. Alper, H. Kockar, JMMM **304**, e784 (2006)
14. A. Tekgül, M. Alper, H. Kockar, J. Mater. Sci. **27**, 10059 (2016)
15. T. Sahin, H. Kockar, M. Alper, J. Supercond. Nov. Magn. **26**, 825 (2013)
16. H. Kuru, H. Kockar, M. Alper, JMMM **444**, 132 (2017)
17. H. Kuru, H. Kockar, M. Alper, J. Mater. Sci. **26**, 5009 (2015)
18. A. Tekgül, H. Kockar, M. Alper, J. Supercond. Nov. Magn. **31**, 2195 (2018)
19. J.H. Miao, T.-T. Fang, H.-Y. Chung, C.-W. Yang, J. Am. Ceram. Soc. **92**, 2762 (2009)
20. T. Durga Rao, A. Kumari, M.K. Niranjan, S. Asthana, Physics B **448**, 267 (2014)
21. B. Kaur, L. Singh, V. Annapu Reddy, D.-Y. Jeong, N. Dabra, J.S. Hundal, Int. J. Electrochem. Sci. **11**, 4120 (2016)
22. A. Ghosh, D.P. Trujillo, H. Choi, S.M. Nakhmanson, S.P. Alpay, J.-X. Zhu, Sci. Rep. **9**, 194 (2019)
23. H. Matsuo, Y. Noguchi, M. Miyayama, Nat. Commun. **8**, 207 (2017)
24. D. Sharma, A. Basantakumar, H. Sharma, Integr. Ferroelectr. **203**, 81 (2019)
25. S.S. Aplesnin, V.V. Kretinin, A.N. Masyugin, O.B. Romanova, M.N. Sitnikov, O.B. Begisheva, A.I. Galyas, O.F. Demidenko, K.I. Yanushkevich, Semicond. Sci. Technol. **34**, 095007 (2019)
26. Q. Xu, H. Zai, D. Wu, T. Qiu, M.X. Xu, Appl. Phys. Lett. **95**, 112510 (2009)
27. Q. Xu, S. Zhou, D. Wu, M. Uhlarz, Y.K. Tang, K. Potzger, M.X. Xu, H. Schmidt, Appl. Phys. **107**, 093920 (2010)
28. K. Chakrabarti, B. Sarakr, V.D. Ashok, S.S. Chauduhari, S.K. De, JMMM **381**, 271 (2015)
29. V.A. Reddy, N.P. Pathak, R. Nath, Solid State Commun. **171**, 40 (2013)
30. M. Safak Haciismailoglu, M. Alper, H. Kockar, J. Electrochem. Soc. **157**, D538 (2010)
31. A. Tekgül, M. Alper, H. Kockar, M. Safak, O. Karaagac, J. Nanosci. Nanotechnol. **10**, 7783 (2010)
32. Y.-L. Zhang, N. Yan, X.-J. Wang, S. Chen, S.-H. Yang, Ferroelectrics **454**, 35 (2013)
33. A.A. Zatsiupa, L.A. Bashkorov, I.O. Troynchuk, G.S. Petrov, A.I. Galyas, L.S. Lobanovsky, S.V. Truhanov, Solid State Chem. **212**, 147 (2014)
34. C.M. Raghavan, D. Do, J.W. Kim, W.-J. Kim, S.S. Kim, J. Am. Ceram. Soc. **95**, 1933 (2012)

35. M. Haciismailoglu, M. Alper, H. Kockar, ECS Trans. **25**, 87 (2010)
36. M.Y. Kagan, K.I. Kugel, Phys. Usp. **44**, 553 (2001)
37. Y. Li, M.B.A. Jalil, S.G. Tan, G. Zhou, Z. Qian, Appl. Phys. Lett. **101**, 262403 (2012)
38. Z. Xu, X. Guo, M. Yao, H. He, L. Miao, J. Lu, H.L.J. Wang, D. Qian, J. Jia, W. Ho, M. Xie, Adv. Mat. **25**, 1557 (2013)
39. H. Kuru, M. Alper, H. Kockar, J. Optoelectron. Adv. Mat. **1**, 432 (2009)